Continental Thunderstorm Ground Enhancement observed at an exceptionally low altitude

Ivana Kolmašová[1,2], Ondřej Santolík[1,2], Jakub Šlegl[3,4], Jana Popová[1], Zbyněk Sokol[1], Petr Zacharov[1],
Ondřej Ploc[3], Gerhard Diendorfer[5], Ronald Langer[6,3], Radek Lán[1], and Igor Strhárský[6]

[1]Institute of Atmospheric Physics of the Czech Academy of Sciences, Prague, Czechia
[2] Faculty of Mathematics and Physics, Charles University, Prague, Czechia
[3] Nuclear Physics Institute of the Czech Academy of Sciences, Husinec-Rez, Czechia
[4] Faculty of Nuclear Sciences and Physical Engineering, Czech Technical University in Prague, Prague, Czechia
[5] Department of ALDIS, OVE Service GmbH, Vienna, Austria
[6] Institute of Experimental Physics, Slovak Academy of Sciences, Kosice, Slovakia

Correspondence to: Ivana Kolmašová (iko@ufa.cas.cz)

Abstract. Two long-lasting Thunderstorm Ground Enhancement (TGE) events were registered at the Milešovka meteorological observatory in Czechia (50.55N, 13.93E, altitude 837 m) on 23 April 2018, during linearly organized thunderstorms. Two intervals of increased photon counts were detected by a plastic scintillator, respectively lasting 70 and 25 minutes, and reaching 31% and 48% above the background radiation levels. Using numerical simulations, we verified that the observed increases of count rates are consistent with the energy spectrum of previously observed TGEs. We investigated the relevant data from a suite of meteorological instruments, a Ka-band cloud radar, an electric field mill, and a broadband electromagnetic receiver, all placed at the Milešovka observatory, in order to analyze the context in which these unique continental TGEs occurred at an exceptionally low altitude. The onset of the TGEs preceded the onset of precipitation by 10 and 3 minutes, respectively, for the two events. Both this delayed rain arrival and a lower energy threshold of 6.5 MeV for registered particles clearly exclude the detection the decay products of the radon progeny washout during the TGE intervals. At the same time, the European lightning detection network EUCLID detected numerous predominantly negative intracloud lightning discharges at distances closer than 5 km from the particle detector, while the occurrence of cloud-to-ground discharges was suppressed. The cloud radar recorded presence of graupel below the melting level and the composition of hydrometeors suggested good conditions for cloud electrification. The observed variations of the near surface electric field were unusual, with very brief negative electric field excursions reaching -20 kV in a quick succession. At the same time, sub-microsecond unipolar pulses emitted by close corona discharges saturated the broadband magnetic loop antenna. All these measurements indicate that a strong lower positive charge region was present inside the thundercloud. The bottom thundercloud dipole was probably responsible for acceleration of the seed electrons in the air. These seed electrons might originate not only in the secondary cosmic ray particles but could also come from a high concentration of radon in the air collected during the propagation of the convective system above the uranium-rich soils before the thunderstorms overpassed the Milešovka observatory.

1 Introduction

"Thunderstorm Ground Enhancement" events are defined as increased fluxes of electrons, neutrons, gamma rays or X rays, which are registered by particle detectors located on the Earth's surface during thunderstorms (Chilingarian et al., 2010, 2011,
40   2015, 2016, 2019; Kudela et al., 2016; Chum et al. 2020). These phenomena are also known as "prolonged radiation bursts" (Tsuchiya et al., 2007), "gamma glows from the ground" (Dwyer et al., 2012), "prolonged gamma ray enhancements" (Shepetov et al., 2021), or "gamma ray bursts" (Brunetti et al., 2000). The first conclusive measurements of these "X-ray enhancements" clearly related to thunderstorms were obtained using airplanes (Parks et al., 1981), followed by "X-ray increases" on balloons (Eack et al., 1996), and by airborne measurements of "gamma ray glows" (Kochkin, 2017; Ostgaard,
45   2019). However, the first theoretical prediction of "extremely penetrating radiation of beta or gamma ray type" was published by Wilson (1925) who hypothesized that beta radiation might come from energetic electrons, accelerated by thunderstorm electric fields from the seed population of decay products of cosmic rays or radionuclides of terrestrial origin, while the gamma component might come from bremsstrahlung after collisions of these electrons with the air molecules. Given the above documented fact, that most papers on this subject coin their proper term to name these interesting phenomena, we have a wide
50   choice of possible names of which we chose the term "Thunderstorm Ground Enhancement (TGE)" which currently occurs most often in the literature.

The main complications for observations of TGEs were (a) emissions originating in the decay chain of the radon washed out from the air by rain and (b) highly absorbing column of the air between the cloud base and the detector (Dwyer et al., 2012).
55   The exclusion of the radon progeny washout and its subsequent decay products (at energies below 3 MeV) in the registered counts started to be possible with an extension of measured particle energies up to 10 MeV. The absorption can be minimized by choosing observational places with a short distance between the cloud base and the detector. This is the reason, why the TGEs were up to now exclusively observed at high mountain observatories (Brunetti et al., 2000; Torii et al, 2009; Chilingarian et al., 2011, 2015, 2016; Kudela et al., 2016; Chum et al. 2020, Shepetov et al., 2021) or at the sea level during Japanese winter
60   storms with extremely low cloud base altitudes (Tsuchiya et al., 2011; Kuroda et al., 2016). Typically, the TGEs last from 1 minute up to 10-15 minutes and the radiation mostly does not exceed 10 % of the background values. Nevertheless, extreme events exceeding several times the background values were also registered (Chilingarian et al., 2010; Chum et al., 2020).

Chilingarian et al. (2012) introduced a two-component model for the TGE generation, which includes the Relativistic Runaway
65   Electron Avalanche (RREA) process originally proposed by Gurevich et al. (1992) and the Modification of electron energy Spectra (MOS) process. RREA might be responsible for multiplication of particle flux up to 10 times above the background of secondary cosmic rays in the energy range up to 30-40 MeV. The MOS process can add only several per cent particle flux to the background values but the energy extends up to 100 MeV. Dwyer and Uman (2014) showed that an avalanche could be produced in the thundercloud electric fields if energetic seed electrons are provided, for example, by secondary cosmic rays.

70 Energetic runaway electrons then generate high-energy photons through the bremsstrahlung interactions with air atoms. These high-energy photons can reach energies of a few tens MeV. A transfer of energy of the thundercloud electric field to the electrons from the ambient population of the cosmic rays leads to a modification of electron energy spectra, to an additional bremsstrahlung, and might be also responsible for the tail of the TGE gamma ray spectra up to 100 MeV (Chilingarian et al., 2012).

75

It was shown by simultaneous measurements of particle fluxes and near surface electric fields that TGEs usually occurred during large values of negative electric fields, which accelerate electrons downwards. Nevertheless, TGEs were rarely detected also during positive electric fields. This can be explained by the asymmetry in the electron/positron component of the secondary cosmic rays (Zhou et al., 2016). TGEs are usually not associated with individual lightning strokes, but sometimes they are
80 terminated abruptly by a nearby lightning discharge (Kudela et al., 2016; Chilingarian et al., 2017a; Chum et al., 2020). TGEs are often observed during time intervals with an increased occurrence of inverted intracloud lightning, which are discharges between the main negative charge region and the lower positive charge region (LPCR), and during a lower occurrence of negative cloud-to-ground (CG) lightning strokes (Chilingarian et al., 2018, 2020). This scenario suggests an existence of a strong LPCR inside the thundercloud, which blocks the propagation of negative leaders down to the ground (Nag and Rakov,
85 2009; Iudin et al., 2017). This arrangement of charges inside the thundercloud also suggests that electrons from the cosmic ray secondaries are accelerated and multiplied in the bottom thundercloud dipole, which is formed by the main negative charge layer and the LPCR (Chilingarian et al., 2017b). This led to a speculation that the intensity of TGEs reached the maximum when the LPCR was directly above the detector and the counts decreased when the cloud moved away. Such movement of clouds would explain a large variety in durations and intensities of the observed TGEs. This effect was reported by Torii et al.
90 (2011), who identified a migrating source of high-energy photons attributed to the thundercloud movement using simultaneous registrations of TGEs, measurements of the near surface atmospheric electric field, and meteorological radar echoes at several points along the Japanese coast.

The mechanism of the LPCR formation is still not fully understood. It is typically located just below the freezing level. Rakov
95 and Uman (2003) proposed several hypothetical sources of positive charge, which can contribute to its accumulation close to the lower cloud boundary. The source of positive charge might be associated with graupels, which are supposed to be positively charged at temperatures warmer than the reversal temperature. Valuable contribution to the LPCR puzzle can be added by information about the thundercloud microphysical structure: a mixture of hydrometeors such as that of graupel, ice, snow and supercooled water is considered prone to cloud electrification (Rakov, 2016). Such data can be delivered by millimeter Doppler
100 polarimetric radars, which investigate the cloud microphysics at high temporal and spatial resolutions (Görsdorf et al., 2015; Kollias et al., 2007; Clothiaux et al., 1995). Positive charge might be also generated by corona discharges at ground level and transferred to an altitude of the cloud base (Chauzy and Soula, 1999). This corona mechanism was also assumed to act as the main contributor to the evolution of the LPCR in the study of Nag and Rakov (2008) who evaluated the role of the LPCR in

facilitating different types of lightning. Electromagnetic pulses emitted by corona discharges might be identified in fast
105 electromagnetic recordings. Arcanjo et al. (2021) found that corona current pulses measured at a shunt resistor have fast rise
times (tens of nanoseconds) and slow decays (hundreds of nanoseconds). They also found that the pulse cadence was correlated
with the ambient electric field measured at a distance of 250 m. Pulses related to positive corona discharges were reported to
be no longer observed for weaker ambient electric fields than -1.8 kV/m. A threshold for negative corona pulses was higher,
reaching about 3.8 kV/m.

110

The first attempt to examine enhancements of gamma ray background, previously attributed solely to radon progeny, was
reported at the territory of Czechia by Šlegl et al. (2019). The authors used the data from the Czech Radiation Monitoring
Network (RMN), which is operated by the State Office for Nuclear Safety, and investigated gamma background enhancements
with respect to the proximity of thunderstorms. They found that increased exposure levels at individual RMN stations observed
115 during close thunderstorms couldn't be explained by the radon progeny itself and suggested that they might have been
attributed also to TGEs.

In the present study, we investigate conditions, which led to the observation of two TGE events detected by a particle detector
at the Milešovka meteorological observatory (Czechia, 837 m a.s.l) on 23 April 2018, using the data collected by a set of
120 instruments: an electric field mill, a broadband electromagnetic receiver, and a Ka-band cloud radar. We combine these
measurements with meteorological data (temperature, precipitation, air pressure, dew point temperature), and with data
provided by the European lightning location network EUCLID. In section 2, we describe the instrumental setup and the dataset.
In section 3, we describe the meteorological situation during the thunderstorms occurring on 23 April 2018. In section 4, we
present results of our analysis of the particle registrations. In section 5, we analyze electrostatic and electromagnetic
125 measurements and investigate characteristics of lightning detected by EUCLID during the analyzed thunderstorms. In section
6, we introduce the relevant observations of the cloud radar. In section 7, we describe the simulation of observed particle
fluxes. In section 8, we discuss and summarize our results.

2 Instrumentation and dataset

The Milešovka meteorological observatory is located on the top of the Milešovka Mt. (a. k. a. Donnersberg, 50.55N, 13.93E,
130 837 m a. s. l.) in Czechia. As it is by 400 meters higher than the surrounding terrain, and has a 360° view unobstructed by
obstacles. Its meteorological and climatological measurements are continuous and date back to 1905. It is known as stormiest
place in the Czech territory.

For registration of particles we use the Space Environment Viewing and Analysis Network (SEVAN) detector described in
135 detail by Chilingarian et al. (2009). The basic SEVAN unit is composed of standard slabs of 50 x 50 x 5 cm3 plastic scintillators.

Between two identical assemblies of 100 x 100 x 5 cm3 scintillators (four standard slabs) are located two 100 x 100 x 5 cm3 lead absorbers and thick 50 x 50 x 25 cm3 scintillator stack (five standard slabs). Scintillator light capture cones and photomultiplier tubes are located on the top, bottom and in the intermediate layers of the detector. The slabs are sealed in a box made of 1 mm thick steel plate. The events described in this study were detected by the middle scintillator stack of SEVAN,

140   which was installed without the shielding lead absorber inside the building of the Milešovka observatory. There was about 80 cm of concrete above the detector and thus a majority of the incoming increased radiation came through the nearby window (see the detailed simulation results in Section 7). The energy threshold for the photomultiplier was set between 6.5 and 7.5 MeV. The counts are stored with a 1-min cadence.

145   The vertical electrostatic field is measured by the electric field mill EFM 100 manufactured by the Boltek Company. The field mill is installed in an inverted position to minimize the noise originating from precipitation. The electric field is sampled at a cadence of 50 ms. Negative values at the field mill output correspond to an upward pointing electric field in which the electrons are accelerated downward.Two perpendicular broadband magnetic loop antennas SLAVIA (Shielded Loop Antenna with a Versatile Integrated Amplifier) are used to measure the time derivative of variations of the horizontal magnetic field from 5

150   kHz up to 90 MHz (Kolmasova et al., 2018, 2020, 2022). The gain of the integrated preamplifiers is remotely controlled. The SLAVIA sensors are coupled with a digital oscilloscope sampling at a frequency of 200 MHz and the digitized signal is numerically integrated. The broadband analyzer is working in a triggered mode based on a predefined amplitude threshold: when it receives a trigger, it records a 168-ms long waveform snapshot including a history of 52 ms. The trigger time is assigned by the GPS receiver with an accuracy of 1 μs. The analyzer triggers on strong signals emitted by different lightning

155   phenomena as return strokes (RS), intracloud (IC) discharges, or preliminary breakdown pulses. In case of a close thunderstorm, it also triggers on very fast sub microsecond pulses radiated by corona-type discharges occurring at the tips of close metallic objects due to the strong electric field below the thundercloud. In this study, we use the measurements of the antenna oriented in the east-west direction.

160   The vertically oriented cloud radar was installed at the Milešovka observatory in 2018. It is a Doppler polarimetric radar (MIRA 35c), which was manufactured and installed by METEK Gmbh (http://metek.de/). It transmits electromagnetic signal within the Ka-band with a center frequency of 35.12 ± 0.1 GHz and a peak power of 2.5 kW. The radar core is of a magnetron type and the radar antenna is of the Cassegrain type with a diameter of 1 m, a gain of 48.5 dB and a beam width of 0.6°. The pulse repetition frequency varies from 2.5-10 kHz and the pulse width from 100 to 400 ns. The unambiguous velocity range

165   ($\pm$ VNyquist) is ± 10.65 m/s. The radar registers Doppler spectra, which correspond to averages of 40 consecutive values above the noise floor. The values below the estimated noise floor are deemed to have no signal. The internal software of the radar provides three moments of the Doppler spectra, such as radar reflectivity (Z), Doppler vertical velocity (DVV) and spectrum width, and derives other quantities such as the linear depolarization ratio (LDR) or signal-to-noise ratio. The temporal resolution of the cloud radar is approximately 2 s, while its vertical resolution covers 509 gates, which are distant by 28.8 m

170   one from another. The method of the hydrometeor classification used in this study was described by Sokol et al. (2018) and its refined version was reported in Sokol et al. (2020). Prior to the hydrometeor classification, we correct the DVV values using the de-aliasing procedure and estimate the vertical air velocity (VAV). The calculation of VAV is based on a common approach according to which the very small particles (i.e. tracers) are so light that they are considered to be carried by the air only, which means that their velocity determines the VAV (Kollias et al., 2001; Gossard, 1994; Shupe et al., 2004). The hydrometeor

175   classification assumes that the terminal velocity varies from one hydrometeor class to another and the hydrometeor classes naturally depend on the ambient air temperature. Based on the ambient air temperature, the terminal velocity range of hydrometeors and the shape of particles determined by LDR, five hydrometeor classes are distinguished in our classification, i.e. cloud liquid water, rain, graupel, hail and ice & snow (Sokol et al., 2020).

3 Thunderstorms on 23 April 2018

180   A cold front belonging to a pressure low over the Norwegian Sea was travelling to Central Europe and replaced a warm central European air mass by a cool maritime polar air. During the day, the CAPE (Convective Available Potential Energy) values gradually increased from almost zero at 00UTC to roughly 800 J.kg 1 at Prague-Libuš (CZ), Mainingen and Kümmersbruck (both DE) sounding stations. The CAPE increase was accompanied by CIN (Convective Inhibition) decrease, which supported the evolution of convective storms. According to the radar measurements from the CZRAD network operated by the Czech

185   Hydrometeorological Institute (Novák, 2007) and EUMETSAT satellite measurements, the morning storms in Germany produced a nicely evolved gust front, which produced a squall line crossing the northwest of the Czech Republic at midday. The origin of the squall line was supported by a direct hodograph with almost no directional shear and a considerable deep layer shear (0-6 km) around 15 m.s 1. The storms crossing the Milešovka observatory in the afternoon were also linearly organized, however, they did not evolve into a squall line like the morning storms. The thunderstorms described in this study

190   occurred around noon (from 10:40 to 13:20 UTC) and in the evening (from 17:00 to 17:50 UTC) and we respectively marked them "storm A" and "storm B". The linear organization of both storms is clearly visible in Fig. 1, where black crosses in both panels show the location of the Milešovka observatory.
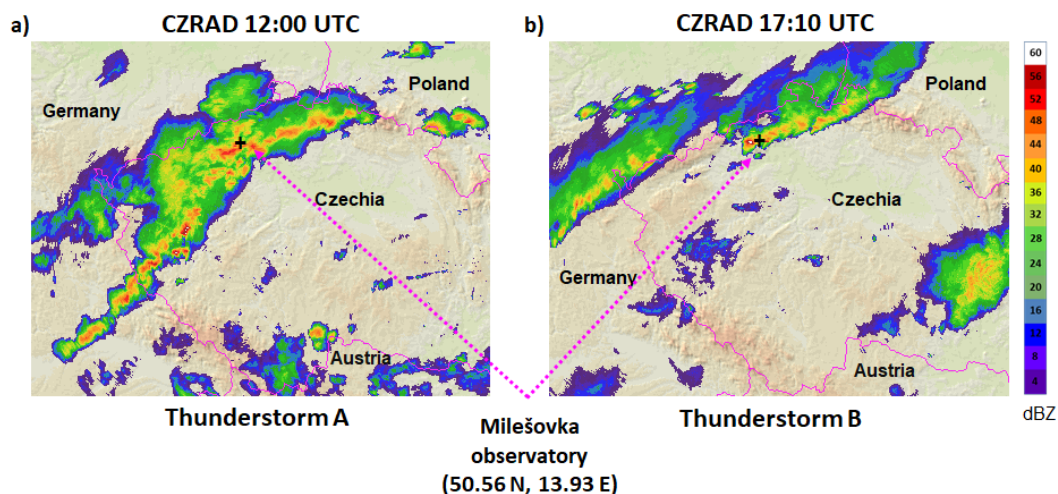
Figure 1: Maps of radar reflectivity for the most intense parts of storm A (a) and storm B (b). Black crosses show location of the Milešovka observatory (source www.chmi.cz on 23 April 2018).

205

The information about the temperature, relative humidity, air pressure, wind speed and its direction, precipitation totals, duration of sunshine and other meteorological parameters is available from the measurements of the automatic Vaisala weather station. For our study, we use the precipitation totals measured in a 1-min cadence, which are shown by blue lines in Figs. 2a and 3a. To estimate an altitude of the cloud base we assume that it in simplicity corresponds to the lifted condensation level

210 (LCL) which we calculated from the temperature at a level of 2 meters and the dew point temperature. Note that this estimation is quite rough as during the precipitation the calculation might be influenced by an increased relative humidity and decreased temperature. Red stars in Figs. 2a and 3a display the altitudes of the LCL above the Milešovka Mt. during both storms. (Note that all altitudes in Figs. 2 and 3 are relative to the altitude of the Milešovka station of 837 m a.s.l). The altitude of the cloud base was respectively estimated to 400 m and 180 m above the detector during storm A and storm B; the 0° C level was located

215 at an altitude of about 2 km above the cloud radar.

4 Particle measurements

The middle scintillator of the SEVAN detector, which was placed close to the window inside the observatory building, detected around 3500 counts/minute during the undisturbed conditions. The count enhancements observed during storms A and B are shown in Figs. 2a and 3a, respectively by black lines. During storm A, the particle counts started to grow at 11:05 UTC,

220 reached a maximum of about 4600 counts/min in 10 minutes, and dropped in the next 10 minutes nearly to the normal count rate. This significant increase of 31 % was later followed by two weaker enhancements of 18 % and 14 %. The fluctuations of the count rate lasted for about 70 minutes. During storm B, the count rate started to grow at 17:10 UTC, reached a maximum of about 5200 particles per minute at 17:23 UTC and dropped to the normal count rate at 17:33 UTC. The maximum count increase was unusually large, reaching 48 %. The precipitation rate shown by blue lines in Figs. 2a and 3a started about 10

225 minutes after the count increase during storm A (Fig. 2a) and about 3-4 minutes later than the count increase in case of the storm B (Fig. 3a). The estimated cloud base was respectively found 200-1100 m and 180-240 m and above the observatory, during the count increases in storm A (Fig. 2a) and storm B (Fig. 3a).

230

235

240

245

250

255

260
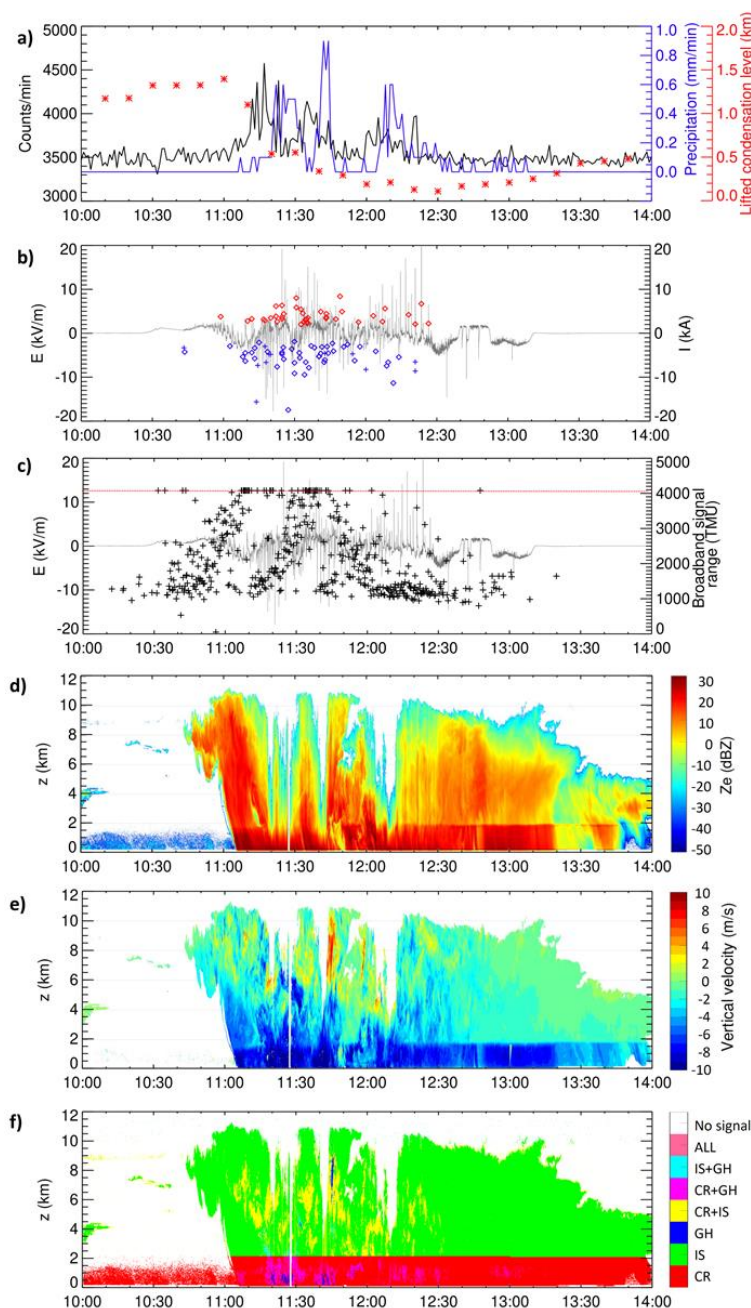
Figure 2: Storm A: a) Particle counts per minute (black line), precipitation totals in mm/min (blue line), the altitudes of the lifted condensation level in km above the altitude of 837 m - Milešovka observatory (red stars); b) fluctuations of the vertical electric field measured by electric field mill (grey line), EUCLID detections: red and blue color for positive and negative discharges, diamonds for IC discharges and crosses for CG discharges; c) fluctuations of the vertical electric field (grey line),

absolute maximum of the range of values measured by the broadband antenna (in telemetry units, each black cross corresponds to the maximum range of the magnetic field derivative recorded during one 168 ms long waveform snapshot), red line shows the saturation in both positive and negative polarity (4096 TMU); d) the radar reflectivity; e) vertical updraft velocity; f) classification of hydrometeors (G-graupel, H-hail, I-ice, S-snow, C-cloud water, R-rain).
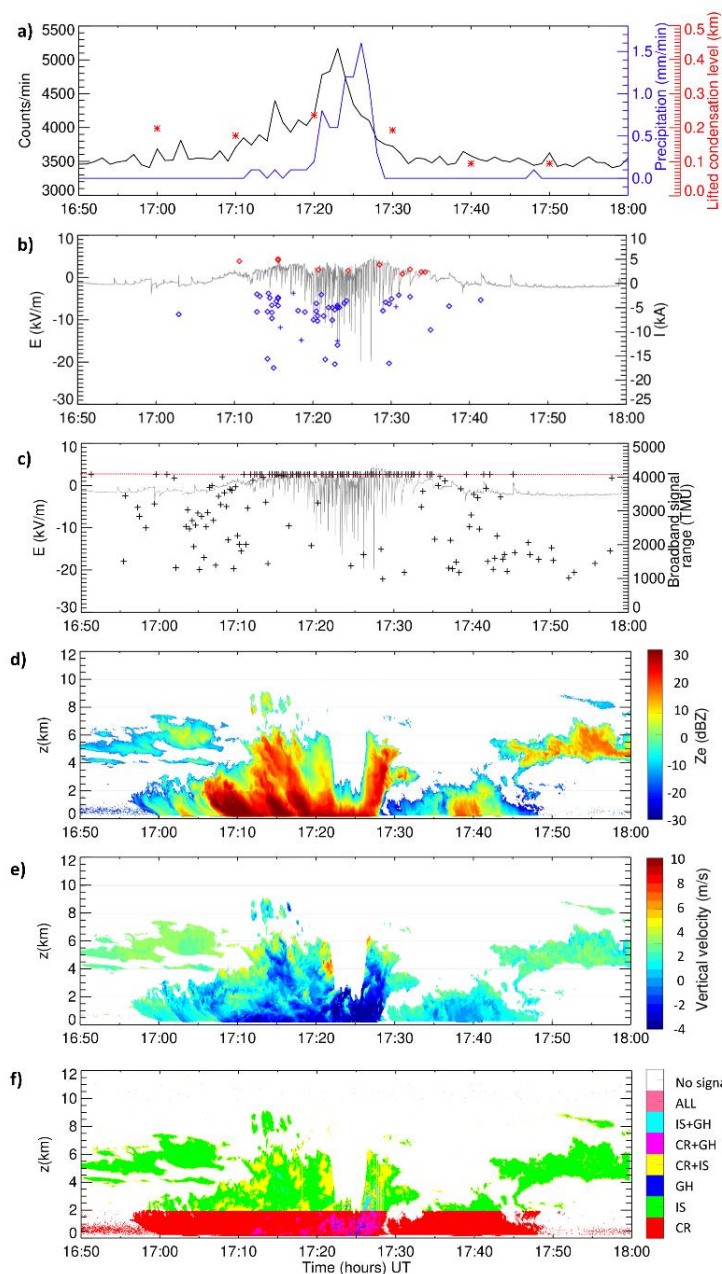
Figure 3: The same as in Fig. 2 but for the storm B.

5 Electromagnetic measurements

5.1 Electric field mill measurement and EUCLID detections

Variations of the atmospheric electric field measured by the electric field mill during the investigated events are shown by

305   grey lines in Figs. 2b, c and 3b, c, respectively. The field mill data show small values of the electric field until 10:45 and since 13:10 during storm A due to the fair-weather current flowing from the ionosphere to the ground. In case of storm B, the electric field waveform exhibited small peaks also before 16:55 and after 17:45. These peaks can be assigned to lightning discharges that occurred more than 5 km away from the sensor. Significant variations of the electric field were detected when the thundercloud was located above the field mill from 10:45 to 13:10 UTC, and from 16:55 to 17:45 UTC, respectively, during

310   storms A and B. The maximum values reached ± 20 kV. Surprisingly, negative peaks in the electric field records dominated until 11:25 during storm A, and only negative pulses were observed during the whole period of storm B. Negative electric field excursions were very short and followed in a quick succession. Such variations of electric fields near the ground are not typical. Rapid changes of polarity in the otherwise slowly varying atmospheric electric field usually correspond to the neutralization of the charge in the thundercloud due to close IC or CG discharges. Detections of the European lightning location network

315   EUCLID, limited up to 5 km from the Milešovka observatory, are displayed in Figs. 2b and 3b by colored symbols. Red and blue crosses are used for positive and negative CG discharges, respectively. Red and blue diamonds show positive and negative IC discharges. The negative sign indicates the movement of the negative charge downward. A substantial lack of CG discharges may be noted. The negative IC discharges, called also inverted IC flashes, were clearly associated with periods of negative excursions of the atmospheric electric field and their occurrence can thus be considered as the primary case of the observed

320   negative peaks. However, inverted IC flashes were detected by EUCLID only for some of observed negative peaks. The amplitudes of negative peaks also clearly do not correspond to the reported peak currents of the inverted IC flashes.

5.2 Broadband magnetic field measurement

The trigger of the broadband analyzer was nearly constantly activated during the time when the thundercloud was located above the observatory. The cadence of the 168-ms long waveform snapshots was mainly given by the ability of the analyzer

325   to store and transfer the data. The maximum amount of 3-4 snapshots per second was reached during the time of the intense variations of the atmospheric electric field. 474 snapshots sampled at 200 MHz were recorded from 10:12 to 13:20 during storm A. During storm B, a set of 159 snapshots was recorded from 17:35 to 17:58.

An example of a waveform snapshot is shown in Fig. 4. The panel 4a displays the complete numerically integrated waveform;

330   panel 4b shows the raw signal measured by the antenna. The waveforms include also a history of 52 ms recorded before the trigger. After the time of the trigger, the signal frequently reached the digital saturation of ± 2040 telemetry units (TMU), when one TMU corresponds to 76 µT/s. As the antenna measures the time derivative of the magnetic field, the repeated saturation indicates very fast changes of the magnetic field. A thorough look at the waveform details reveals that the records are composed

from a mixture of pulses of different shapes, widths, and polarities. This mixture is not surprising: the analyzer is able to detect

335 the RS pulses and IC pulses occurring a few hundreds of kilometers from their causative discharge and in case of a very close storm it is often saturated by fast pulses emitted by corona discharges appearing at the tips of close metallic objects. Fast unipolar pulses with a width of a few tens of nanoseconds which originated in close corona discharges are shown in Figs. 4c and 4f.
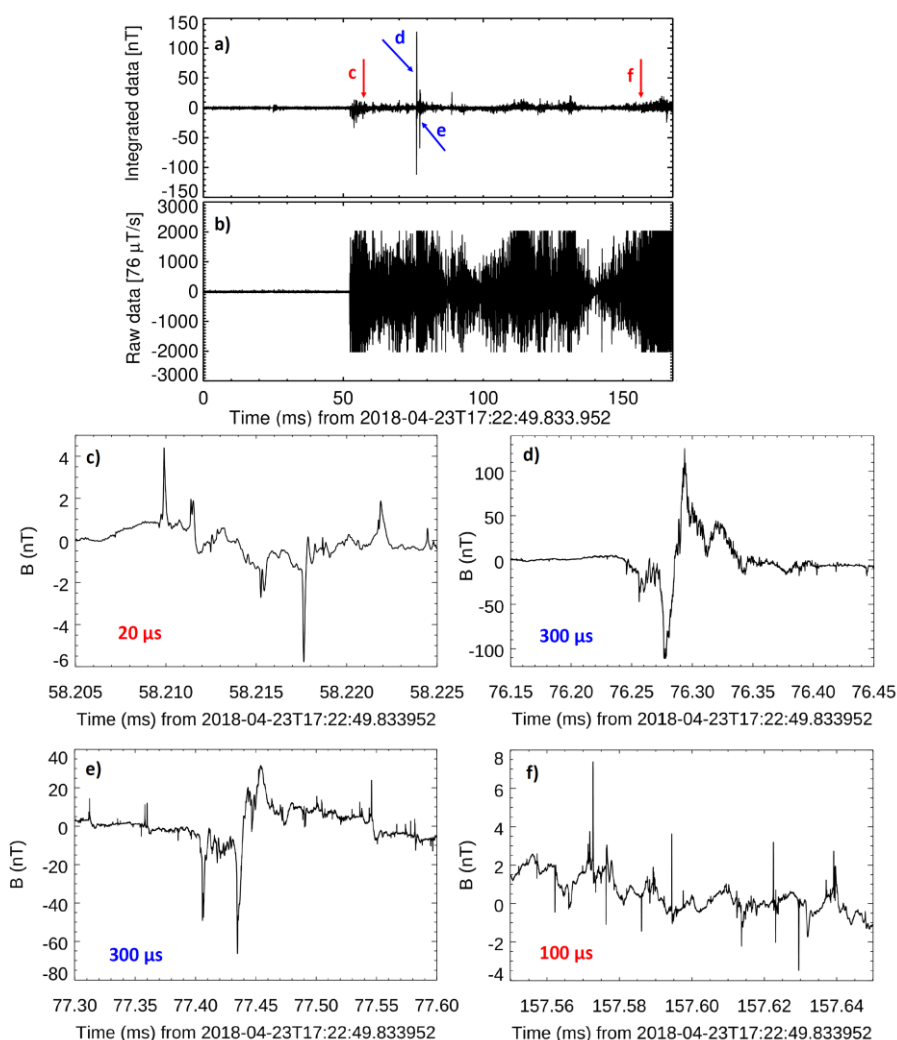
340 **Figure. 4:** Example of a 168-ms long magnetic field waveform snapshot measured by a broadband antenna: a) integrated magnetic field waveform; b) the time derivative of the magnetic field fluctuations, the trigger was activated at 52 ms; c-f) 20-300 μs long details indicated by arrows in the panel a: c) submicrosecond unipolar pulses emitted by corona discharges; d) a bipolar pulse emitted probably by a strong close IC discharge; e) a RS type pulse; f) mixture of different pulses.

345 The rapidly changing polarity either indicates that the corona discharges arose at different directions with respect to the axis of the magnetic loop antenna, or that both negative and positive corona discharges occurred. We are not able to distinguish between these two possibilities by our measurements. Fig. 4d shows an intense bipolar pulse at 76.24 ms emitted probably by a close IC discharge. A typical RS pulse is recognizable in Fig. 4e at 77.43 ms and might have been generated by a distant CG discharge.

350

All waveform snapshots are composed of a mixture of pulses and a large part of snapshots recorded during active parts of both storms reached the negative, positive or both digital saturation levels. We therefore calculated the maximum range of measured raw values for all 633 waveform snapshots. The obtained values are plotted by black crosses in Figs. 2c and 3c. The maximum range of 4080 TMU is represented by red solid lines. It is clearly visible that during intense negative excursions of the

355 atmospheric field during storm B saturation was reached during nearly all recorded waveform snapshots.

6 Cloud profiler measurements

6.1 Storm A

Figure 2d shows the time evolution of the radar reflectivity factor, which we measured by the cloud radar, during the first thunderstorm event (11-14 UTC approximately). It clearly depicts that the values of reflectivity, especially during the first half

360 of the event, reaches or exceeds 30 dB in most of the vertical profile. The vertical extent is up to 10 km suggesting a vertically developed thundercloud situated above the Milešovka observatory. Based on high reflectivity values, we can assume that the melting layer was at a height of 2 km above the radar approximately and that up to 13:20 UTC precipitation occurred in lower elevations. The lower reflectivity values during the second half of the event represents the rear part of the squall line where slighter precipitation than in the front part is located. Figure 2e displays the time evolution of DVV, where the upward motion

365 is depicted by positive values while the downward motion by negative values. Positive values, i.e. upward motion, prevails in upper elevations, while negative values, i.e. downward motion, dominates lower elevations and suggest fall out of greater (i.e. precipitation) particles. Hydrometeor distribution as it resulted from the algorithm by Sokol et al. (2020) during the first thunderstorm event is depicted in Figure 2f. Naturally, most of the higher elevations consist of ice and snow, while the lower elevations consist of liquid cloud water and rain. However, it is worth noting that during the first half of the event, we also

370 detected graupel and hail in the lowest elevations, which can be related to heavy precipitation. Interestingly, from about 5 to 9 km above the radar at 11:45 approximately, there is a mixture of graupel and hail surrounded by ice and snow and supercooled liquid cloud water. This might be a place where the process of cloud electrification could be expected according to the widely accepted theory of cloud electrification by collisions of graupel with ice and snow particles in presence of supercooled cloud liquid water.

6.2 Storm B

Figure 3d shows the time evolution of the measured radar reflectivity by the cloud radar during the second thunderstorm event. As compared to the first thunderstorm event, it is obvious that the vertical extent of the cloud during the second thunderstorm event is much lower, up to 6 km above the radar approximately. This may be related to the fact that the cloud radar is only vertically pointing and thus does not see the whole thundercloud horizontally. In the case of this thunderstorm, the cloud radar likely scanned a side part of the thunderstorm instead of its core, as you can see on Figure 1b. However, the radar reflectivity values are as high as during the first thunderstorm event suggesting a possible fallout of precipitation. The melting height is hardly definable in this case. The gap in measurements from 17:20 to 17:30 UTC from about 2 to 6 km can either be related to attenuation of the radar signal by heavy rain but the reflectivity values are pretty low or simply and more likely it corresponds to the fact that the cloud was not that extensive at that time. The time evolution of DVV is displayed in Fig. 3e. In contrary to the first thunderstorm event, the upward motion reaches lower values in general, while the downward motion is similar to the first event, suggesting precipitation fallout. As far as the hydrometeor distribution during the second thunderstorm event is concerned, Fig. 3f shows the time from 17:20 to 17:30 the most interesting as all the hydrometeor classes were detected at that time, though the cloud is too low to draw any conclusions out of it. Further, the distribution is expectable and similar to the first event with e.g., a predominance of cloud water and rain at the lowest elevations.

7 Simulation of particle fluxes

The installation of the particle detector SEVAN was not the same as for other measurements sites and the obtained counts thus are not directly comparable with the existing TGE reports. We therefore verify the enhancement of counts in our detector for a known TGE energy spectrum (Chilingarian and Mailyan, 2013) using the PHITS (Particle and Heavy Ion Transport code System) Monte Carlo based program for particle transport simulations. We use the version 3.24 released in 2021 together with the INCL, EGS5, and KUROTAMA models. We also used the PHITS Cosmic-ray source mode based on PARMA/EXPACS (Sato et al., 2018; Boudard et al., 2013; Iida et al., 2007; Sato, 2015, 2016).

The geometry of the detector installation inside the observatory building is simplified as an inner space of air with dimensions of 4 x 4 x 3 m in x, y, and z axes (where z is vertical pointing up), surrounded by concrete walls with a width of 80 cm. At a height of 1 m there is a 1 m high window opening with a width of 0.5 m. The opening is filled with a 2 mm thick glass. The sensitive volume of plastic scintillator with the dimensions of 50 x 50 x 25 cm3 is placed at a distance of 40 cm from the window and 100 cm above the floor. The scintillator is covered with a 1 mm thick steel plate, which represents the scintillator box. On the top of the concrete ceiling, a wooden plate with a thickness of 3 cm and a steel plate with a thickness of 1 mm represent the roof. This environment is visible as a black rectangular shape in Fig. 5a.

As the first step, we test our setup by comparing measured and calculated background count rates originating in the secondary cosmic ray particles. The measured background rate was around 3500 counts/minute (Figs. 2a and 3a). The PHITS's cosmic rays source for the specific date and height gives us a total number of 3640 ± 135 counts/minute for the energy higher than 6.5 MeV deposited in the scintillator (3432 ± 118 muons/minutes, the rest include electrons/positrons, photons and neutrons). The

410 calculated count fits well the observation.
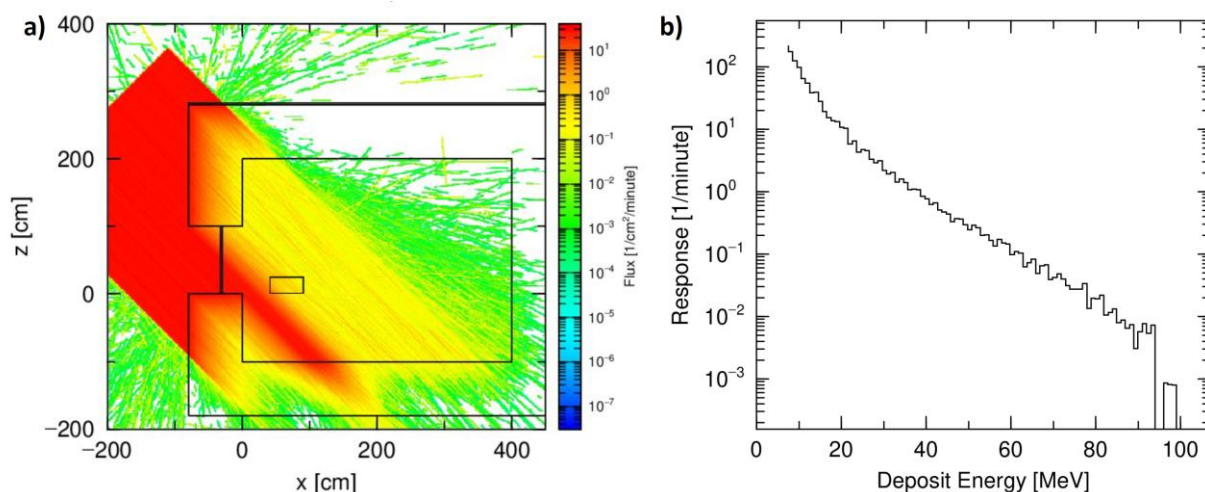
Figure 5: a) TGE source particles, the source is tilted by 45° from the vertical axis, and the energy spectra correspond observation by Chilingarian and Mailyan (2013). b) Deposit energy spectra inside the scintillator. Lower energy threshold was set to 6.5 MeV according to the setup of the detector.

425 As we do not measure the energetic spectrum for the TGE events observed at Milešovka, we use a known TGE spectrum measured at the Aragats observatory on 4 October 2010 when the count enhancement in the upper SEVAN scintillator reached of about 34 % (Chilingarian & Mailyan, 2013), similarly to our observation. The source geometry is represented by a square of 3 x 3 m2 located at a distance of 3 meters from the detector in order to minimize the influence of scattered particles. The direction of the particle beam is perpendicular to the source plate and the detector is approximately in the middle of the beam.

430 The dead time of the detector is not taken into account due to the fast response of the plastic scintillator and due to the very high energy threshold. The source is composed only from photons. The electrons are not included, as their ability to cross the concrete walls or the window, and to deposit enough energy in the scintillator is negligible. According to Chilingarian & Mailyan (2013), the photon differential intensity I in particles/min/MeV/m2 can be represented as $I = 4.5 \times 10^5 \, e^{-(0.25 \, E/MeV)}$ for photon energies E from 5 to 10 MeV, and $I = 6.3 \times 10^7 \, e^{-(3.3 \, E/MeV)}$ for photon energies E from 10 to 100 MeV. By

435 integrating the spectrum over all energies, we get the total number of photons in the source equal to 5.05 x 10^5 per minute and m2. If we place the photon source on the top of the simulated environment, slant it by 45° to let the particles enter the window, the area of the detector (small box at coordinates x=50, z=0 in Fig. 5a) is hit by approximately one source particle/cm2/minute.

The surface of the detector perpendicular to the beam is 2652 cm². The spectrum of particle energies absorbed in the scintillator and originating solely from the TGE source (without cosmic rays) is shown in Fig.5b. The count rate of particles with an

440   energy range from 6.5 to 100 MeV deposited in the detector can be estimated using the T-deposit tally as (977 ± 3)/min. This number represents a 27% increase of the count rates relative to the background, which is roughly consistent with the observed peak count rates (31% and 48%, respectively, for storm A and storm B in Fig. 2a and 3a). The slightly higher observed fluxes can be likely explained by stronger source particle fluxes in our case compared to the case analyzed by Chilingarian & Mailyan (2013) or by inaccuracies of the event geometry in our model.

7 Discussion and summary

Two significant TGE events were registered on 23 April 2018 at the Milešovka observatory in Czechia at 837 m a.s.l. To our best knowledge, it was the first multi-instrument TGE observation below 1 km above the sea level outside Japan. The registered increases of photon count reached 31 % and 48 % above the background level during the thunderstorms A and B, respectively. The duration of TGEs was unusually long in comparison with other reports (Chum et al., 2020; Chilingarian et al. 2017 a,b,

450   2020), lasting about 70 minutes (storm A) and about 25 min (storm B). The increased counts were detected by a plastic scintillator of the particle detector SEVAN (Chilingarian et al., 2009). Rain appeared with a delay of several minutes after the count increases during both events.

This delayed rain arrival and an energy threshold of 6.5 MeV for registered particles in the scintillator clearly exclude the

455   presence of the radon progeny washout and its subsequent decay in the count rates. Using the simulations, we verified that the observed increases of count rates can be related to TGEs. We also verified that no extreme cosmic ray events were detected during these observations (https://gle.oulu.fi/#/).

A question, however, remains, why only these two TGE events were registered at the Milešovka observatory, while the particle

460   measurement was operational also in the thunderstorm seasons 2020 and 2021. Based on long-term observations (Kašpar et al., 2018), meteorological data from 23 April 2018 do not indicate any extreme weather event. The TGE events were observed during two convective storms with well-organized multi-cells, but neither precipitation totals (Fig. 2a, 3a) nor the maximum wind speed of 14 m/s exceeded values observed during numerous thunderstorms occurring in the same area in 2020 and 2021. The observatory was not inside the thundercloud as it was the case of TGEs observed at the high mountain observatory (Chum

465   et al., 2020). The cloud base was respectively found at least 200 m and 180m above the observatory during the storm A and B. The 0°C level was located at an altitude of about 2 km above the cloud radar. An estimated height of the cloud tops during the storm A was about 11 km (Figs. 2d-f), as expected in the midlatitudes. The cloud tops during storm B were lower, at about 8 km (Figs. 3d-f), indicating that the storm center of the second storm was not directly above the cloud radar. The updraft velocities reached typical values of 10 m/s. During both storms, the cloud radar recognized graupel below the melting level.

470 Based on the classification of the hydrometeors using the Ka-band cloud radar data, the composition of hydrometeors suggested good but not extreme conditions for the cloud electrification.

Analysis of electromagnetic measurements (broadband magnetic-field data, records of the vertical electric field monitor and EUCLID lightning detections) reveals several interesting characteristics of the investigated thunderstorms. Variations of near

475 surface electric fields observed during both storms were very different compared to previous observations during TGE events, reported for example by Chum et al., (2020), Chilingarian (2017b, 2020). Typically, large and slowly varying negative (but sometimes also positive) electric field was measured in the time interval during which a TGE event was observed. An abrupt decrease of the TGE counts often coincided with a sudden polarity change of the electric field, induced by a lightning discharge. Both positive and negative CG or IC discharges were observed to terminate the TGE events. In our case, the data showed a

480 completely untypical behaviour: negative electric field excursions were very short and followed each other in a quick succession. Some of them were associated with inverted IC strokes detected by EUCLID, none of which, however, abruptly terminated the TGE flux. A frequent occurrence of IC lightning with and a low occurrence of CG lightning indicate a presence of a strong lower positive charge region. The increases of the TGE radiation corresponded in time to the frequent occurrence of large negative pulses electric fields (up to – 20 kV/m) corresponding most probably to inverted IC strokes. We also identified

485 numerous sub-microsecond-scale pulses in the broadband magnetic field records, which often saturated the preamplifier (Fig. 4b), and can be attributed to corona-type discharges occurring at close metallic objects near the receiving antenna in high local electric fields below the thundercloud. These fast unipolar, a few tens of nanoseconds wide pulses (shown in detail in Figs. 4e) are similar to pulses emitted by corona discharges in Arcanjo et al. (2021). Unlike Arcanjo et al. (2021) we cannot distinguish between pulses emitted by positive and negative corona, as their polarity is dependent not only on the direction of the corona

490 current but also on the relative orientation of the magnetic loop to the source discharge. Based on the simulation by Kašpar et al. (2015) the unipolar character of pulses indicates a high propagation velocity of the current waves or short discharge channels or both, which is consistent with expected properties of corona-type discharges.

All electromagnetic measurements indicate a presence of a strong LPCR:

a. an increased occurrence of inverted IC lightning,

495 b. a suppressed occurrence of CG lighting,

c. a presence of strong corona discharges which might have been contributing to the delivery of additional positive charge to the cloud base.

Moreover, the cloud radar identified graupel, which are supposed to carry positive charge at temperatures above the melting

500 level (Takahashi, 1978). This LPCR inside the thundercloud is probably responsible for a high electric field in the bottom thundercloud dipole, which accelerated seed electrons and as a result, we observed significant long-lasting bremsstrahlung.

The exceptionality of the observation rises a question if the secondary cosmic ray particles, which might have been substantially attenuated at the altitude of the observatory, were the only source of the seed electrons. It is possible that

substantial a part of the seed electrons might have originated in a high concentration of radon in the air collected above the uranium-rich soils during rainless period before the thunderstorms overpassed the area (https://remap.jrc.ec.europa.eu/Atlas.aspx#).

In summary, our multi-instrument data recorded during two continental thunderstorms on 23 April 2018 reveal that TGEs can occur at an altitude lower than 1 km above the sea level. The uniqueness of these TGE registrations implicates the idea that the observational conditions might have been unusually favourable. The meteorological situation allowed for a formation of a strong lower positive charge region located close to the observatory (only 180 m above it during the storm B). The presence of lower positive charge region was indirectly confirmed by the electromagnetic measurements, with a possible contribution from local corona discharges, and by the cloud radar data. The bottom thundercloud dipole was probably capable to accelerate the seed electrons in the air. These seed electrons might, besides the usually considered source from the secondary cosmic rays, also originate from radon in the air collected in this specific region.

Data availability

The electromagnetic data are available at http://bleska.ufa.cas.cz/ml/. Particle data are available at http://sevan.ufa.cas.cz/.

Author contribution

IK and OS designed the study and interpreted the results. JS and OP analysed the particle data and performed the flux simulations. JP and ZB analysed and interpreted the cloud profiler data. PZ described the meteorological context. GD provided the EUCLID data. RaL, RoL and IS were responsible for the instrumentation and data storage. The paper was written by IK, OS, JP and PZ.

Competing interests

The authors declare that they have no competing interests.

Acknowledgements

The work was supported by the GACR grant 20-09671S and by the European Regional Development Fund-Project CRREAT (CZ.02.1.01/0.0/0.0/15_003/0000481).

References

530   Alexeenko, V. V., Khaerdinov, N. S., Lidvansky, A. A., and Petkov, V. B.: Transient variations of secondary cosmic rays due to atmospheric electric field and evidence for pre-lightning particle acceleration. Physics Letters A, 301(3-4), 299-306, 2002.

Arcanjo, M., Montanyà, J., Urbani, M., Lorenzo, and V., Pineda: Atmospheric Research 247, 105238, 2021.

Boudard, A., Cugnon, J., David, J.-C., Leray, S. and Mancusi, D.: New potentialities of the Liège intranuclear cascade model
535   for reactions induced by nucleons and light charged particles, Phys. Rev C87, 014606, doi:10.1103/PhysRevC.87.014606, 2013.

Brunetti, M., Cecchini, S., Galli, M., Giovannini, G., and Pagliarin, A.: Gamma-ray bursts of atmospheric origin in the MeV energy range Geophys. Res. Lett. 27, 1599–1602. doi:10.1029/2000GL003750, 2000.

Chauzy, S. and Soula, S.: Contribution of the ground corona ions to the convective charging mechanism, Atmospheric
540   Research, 51, 279–300, 1999.

Chilingarian, A., Hovsepyan, G., Arakelyan, K., Chilingaryan, S., Danielyan, V., Avakyan, K., … Tserunyan, S.: Space environmental viewing and analysis network (SEVAN), Earth, Moon and Planets, Vol. 104, pp. 195–210, doi:10.1007/s11038-008-9288-1, 2009.

Chilingarian A., Daryan, A., Arakelyan, K., Hovhannisyan, A., Mailyan, B., Melkumyan, L., Hovsepyan, G.: Ground-based
545   observations of thunderstorm correlated fluxes of high-energy electrons, gamma rays, and neutrons. Phys Rev D. 82:043009, 2010.

Chilingarian, A., Hovsepyan, G., and Hovhannisyan, A.: Particle bursts from thunderclouds: Natural particle accelerators above our heads. Physical Review D, 83. 062001, 2011.

Chilingarian, A., Mailyan, B., and Vanyan, L.: Recovering of the energy spectra of electrons and gamma rays coming from
550   the thunderclouds, Atmospheric Research 114–115, doi:0.1016/j.atmosres.2012.05.008, 2012.

Chilingarian, A., Soghomonyan, S., Khanikyanc, Y., and Pokhsraryan, D.: On the origin of particle fluxes from thunderclouds, Astroparticle Physics, 105, 54–62, doi: 0.1016/j.astropartphys.2018.10.004, 2019.

Chilingarian, A., Chilingaryan, S., and Reymers, A.: Atmospheric discharges and particle fluxes, J. Geophys. Res. Space Physics, 120, 5845–5853, doi:10.1002/2015JA021259, 2015.
555   Chilingarian, A., Hovsepyan, G. and Kozliner, L.: Extensive air showers, lightning, and hunderstorm ground enhancements, Astroparticle Physics 82, 21, 2016.

Chilingarian, A., Chilingaryan, S., Karapetyan, T., Kozliner, L., Khanikyants, Y. Hovsepyan, G., Pokhsraryan, D., and Soghomonyan, S.: On the initiation of lightning in thunderclouds, Scientific Reports, 7, doi:10.1038/s41598-017-01288-0, 2017a.

560 Chilingarian, A. Khanikyants, Y., Mareev, E., Pokhsraryan, D., Rakov, V. A., and Soghomonyan, S.: Types of lightning discharges that abruptly terminate enhanced fluxes of energetic radiation and particles observed at ground level, J. Geophys. Res. Atmos. 122, 7582, 2017b.

Chilingarian, A., Hovsepyan, G., Soghomonyan, S. Zazyan, M., and Zelenyy, M.: Structures of the intracloud electric field supporting origin of long-lasting thunderstorm ground enhancements, Physical review D 98, 082001,

565 doi:10.1103/PhysRevD.98.082001, 2018.

Chilingarian, A., Khanikyants, Y., Rakov, V. A., and Soghomonyan, S.: Termination of thunderstorm-related bursts of energetic radiation and particles by inverted intracloud and hybrid lightning discharges. Atmospheric Research, 233, 104713, 2020.

Chum, J., Langer, R., Baše, J., Kollárik, M., Strhárský, I., Diendorfer, G., and Rusz, J.: Significant enhancements of

570 secondary cosmic rays and electric field at the high mountain peak of Lomnický Štít in High Tatras during thunderstorms, Earth, Planets and Space, 72:28, doi:10.1186/s40623-020-01155-9, 2020.

Clothiaux, E. E., Miller, M. A., Albrecht, B. A., Ackerman, T. P., Verlinde, J., Babb, D. M., Peters, R. M., and Syrett, W. J.: An Evaluation of a 94-GHz Radar for Remote Sensing of Cloud Properties. J. Atmos. Ocean. Technol. 12, 201–229, 1995.

Dwyer, J. R., Smith, D. M., and Cummer, S. A.: High-energy atmospheric physics: Terrestrial gamma-ray flashes and related

575 phenomena. Space Science Reviews, 173, 133–196,doi:10.1007/s11214-012-9894-0, 2012.

Dwyer J. R., and Uman, M. A.: The physics of lightning. Phys Rep 534, pp. 147–241, doi: 10.1016/j.physrep.2013.09.004., 2014.

Eack, K. B., Beasley, W. H., Rust, W. D., Marshall, T. C., and Stolzenburg, M.: Initial results from simultaneous observation of X-rays and electric fields in a thunderstorm. Journal of Geophysical Research, 101(D23), 29,637–29,640,

580 doi:10.1029/96JD01705, 1996.

Görsdorf, U., Lehmann, V., Bauer-Pfundstein, M., Peters, G., Vavriv, D., Vinogradov, V.and Volkov, V.: A 35-GHz Polarimetric Doppler Radar for Long-Term Observations of Cloud Parameters—Description of System and Data Processing. J. Atmos. Ocean. Technol. 32, 675–690, 2015.

Gossard, E. E.: Measurement of Cloud Droplet Size Spectra by Doppler Radar. J. Atmos. Ocean. Technol. 11, 712–726,

585 1994.

Gurevich, A. V., Milikh, G. M., and Roussel-Dupre, R.: Runaway electron mechanism of air breakdown and preconditioning during a thunderstorm, Phys. Lett. A, 165, 463 – 468, 1992.

Hirayama, H, Namito, Y., Bielajew, A. F., Wilderman, S. J., and Nelson, W. R. : SLAC-R-730 and KEK Report 2005-8 documented in the EGS5 Code System, 2005.

590 Iida, K., Kohama, A., and Oyamatsu, K. Formula for Proton–Nucleus Reaction Cross Section at Intermediate Energies and Its Application, J. Phys. Soc. Japan 76, 044201, doi:10.1143/JPSJ.76.044201, 2007.

Iudin, D. I., Rakov, V. A. , Mareev, E. A., Iudin, F. D., Syssoev, A. A., and Davydenko, S. S.: Advanced numerical model of lightning development: Application to studying the role of LPCR in determining lightning type, J. Geophys. Res. Atmos., 122, 6416–6430, doi:10.1002/2016JD026261, 2017.

595 Kašpar, M., Müller, M., Crhová, L., E., Polášek, J. F., Pop, L., and Valeriánová, A.: Relationship between Czech windstorms and air temperature. Int. J. Climatol., 37, 11–24, doi: 10.1002/joc.4682, 2017.

Kašpar, P., Santolík, O., and Kolmašová, I.: Unipolar and bipolar pulses emitted during the development of lightning flashes, Geophys. Res. Lett., 42, doi:10.1002/2015GL064777, 2015.

Kochkin, P., van Deursen, A. P. J., Marisaldi, M., Ursi, A., de Boer, A. I., Bardet, .,… and Østgaard, N.: In-flight observation
600 of gamma ray glows by ILDAS. Journal of Geophysical Research: Atmospheres, 122, 12,801–12,811, doi:10.1002/2017JD027405, 2017.

Kollias, P., Albrecht, B.A., Lhermitte, R., and Savtchenko: A. Radar Observations of Updrafts, Downdrafts, and Turbulence in Fair-Weather Cumuli. J. Atmos. Sci. 58, 1750–1766, 2001.

Kollias, P., Clothiaux, E. E., Miller, M. A., Albrecht, B. A., Stephens, G. L., and Ackerman, T. P.: Millimeter-Wavelength
605 Radars: New Frontier in Atmospheric Cloud and Precipitation Research. Bull. Am. Meteorol. Soc. 88, 1608–1624, 2007.

Kolmašová, I., Santolík, O., Defer, E., Kašpar, P., Kolínská, A., Pedeboy, S., and Coquillat, S.: Two propagation scenarios of isolated breakdown lightning processes in failed negative cloud-to-ground flashes. Geophysical Research Letters, 47, doi:10.1029/2020GL090593, 2020.

Kolmašová, I., Santolík, O., Defer, E., Rison, W., Coquillat, S., Pedeboy, S. et al.: Lightning initiation: Strong VHF radiation
610 sources accompanying preliminary breakdown pulses during lightning initiation, Scientific Reports, volume 8, Article number: 3650, doi:10.1038/s41598-018-21972-z, 2018.

Kolmašová, I., Soula, S., Santolík, O., Farges, T., Bousquet, O., Diendorfer, G., et al.: A frontal thunderstorm with several multi-cell lines found to produce energetic preliminary breakdown. Journal of Geophysical Research: Atmospheres, 127, doi:10.1029/2021JD035780, 2022.

615 Kuroda, Y., Oguri, S., Kato, Y., Nakata, R., Inoue, Y., Ito, C., and Minowa, M.: Observation of gamma ray bursts at ground level under the thunderclouds, Physics Letters B, 758, 286–291, doi: 10.1016/j.physletb.2016.05.029, 2016.

Nag, A., and Rakov, V. A.: Some inferences on the role of lower positive chargé region in facilitating different types of lightning. Geophysical Research Letters, 36(5), 2009.

Novák, P.: The Czech Hydrometeorological Institute's severe storm nowcasting systém, Atmos. Res., 83(2):450-457,
620 doi:10.1016/j.atmosres.2005.09.014, 2007.

Østgaard, N., Christian, H. J., Grove, J. E., Sarria, D., Mezentsev, A., Kochkin, P., et al.: Gamma ray glow observations at 20-km altitude. Journal of Geophysical Research: Atmospheres, 124, 7236–7254, doi:10.1029/2019JD030312, 2019.

Parks, G., Mauk, K. B. H., Spiger, R, and Chin, J.: X-ray enhancements detected during thunderstorm and lightning activities, Geophys. Res. Lett, 8, 11, 1176-1179, 1981.

625 Rakov, V. A.: Fundamentals of Lightning, Cambridge University Press, Cambridge, UK, ISBN 978-1-107-07223-7, 2016.

Sato, T.: Analytical Model for Estimating Terrestrial Cosmic Ray Fluxes Nearly Anytime and Anywhere in the World: Extension of PARMA/EXPACS, PLOS ONE 10(12), doi: 10.1371/journal.pone.0144679, 2015.

Sato, T.: Analytical Model for Estimating the Zenith Angle Dependence of Terrestrial Cosmic Ray Fluxes. PLOS ONE 11(8), doi 10.1371/journal.pone.0160390, 2016.

630 Sato, T., Iwamoto, Y., Hashimoto, S., Ogawa, T., Furuta, T. et al.: Features of Particle and Heavy Ion Transport code System (PHITS) version 3.02, J.Nucl.Sci.Technol.55, 684-690, doi:10.1080/00223131.2017.1419890, 2018.

Shepetov, A., Antonova, V., Kalikulov, O. Kryakunova, O., Karashtin, A., Lutsenko, V., Mamina, S., Mukashev, K., Piscal, V., Ptitsyn, M., Ryabov, V., Sadykov, T., Saduev, N. Salikhov, N., Shlyugaev, Y., Vildanova, L., Zhukov, V., Gurevich, A: The prolonged gamma ray enhancement and the short radiation burst events observed in thunderstorms at Tien Shan,

635 Atmospheric Research 248, doi:10.1016/j.atmosres.2020.105266, 2021.

Shupe, M. D., Kollias, P., Matrosov, S.Y., and Schneider, T.L.: Deriving Mixed-Phase Cloud Properties from Doppler Radar Spectra. J. Atmos. Ocean. Technol. 21, 660–670, 2004.

Šlegl, J., Minářová, J., Kuča, P., Kolmašová, I., Santolík, O., Sokol, Z., ... and Ploc, O.: Response of the Czech RMN network to thunderstorm activity. Radiation protection dosimetry, 186(2-3), 215-218, 2019.

640 Sokol, Z., Minářová, J., and Fišer O.: Hydrometeor Distribution and Linear Depolarization Ratio in Thunderstorms. Remote Sensing, 12, 2144, doi:10.3390/rs12132144, 2020.

Sokol, Z., Minářová, J., and Novák, P.: Classification of Hydrometeors Using Measurements of the Ka-Band Cloud Radar Installed at the Milešovka Mountain (Central Europe). Remote Sensing, 10, 1674, doi:10.3390/rs10111674, 2018.

Takahashi, T.: Riming Electrification as a Charge Generation Mechanism in Thunderstorms, Journal of the Atmospheric

645 Sciences, doi:10.1175/1520-0469(1978)035<1536:REAACG>2.0.CO;2, 1978.

Torii, T., Sugita, T., Tanabe, S., Kimura, Y., Kamogawa, M., Yajima, K., and Yasuda, H.: Gradual increase of energetic radiation associated with thunderstorm activity at the top of Mt. Fuji, Geophys. Res. Lett., 36, L13804, doi:10.1029/2008GL037105, 2009.

Tsuchiya, H., Enoto, T., Yamada, S., Yuasa, T., Nakazawa, K., Kitaguchi, T.,…Makishima, K.: Long duration γ ray

650 emissions from 2007 and 2008 winter thunderstorms. Journal of Geophysical Research, 116, D09113, doi: 10.1029/2010JD015161, 2011.

Wilson, C. T. R. The acceleration of particles in strong electric fields such as those of thunderclouds, Proc. Cambridge Philos. Soc., 22, 534-538, 1925.

Zhou, X. X., Wang, X. J., Huang, D. H., and Jia, H. Y.: Effect of near-earth thunderstorms electric field on the intensity of

655 ground cosmic ray positrons/electrons in Tibet. Astroparticle Physics, 84, 107–114, doi:10.1016/j.astropartphys.2016.08.004, 2016.